RSC Advances

ROYAL SOCIETY OF CHEMISTRY

www.rsc.org/advances

Cite this: DOI: 10.1039/c0xx00000x

www.rsc.org/xxxxxx

FULL PAPER

Study of Glycine Nitrate precursor method for synthesis of Gadolinium doped Ceria ($Ce_{0.8}Gd_{0.2}O_{1.90}$) as electrolyte for intermediate temperature solid oxide fuel cells

Shrikant Kulkarni [a], Siddhartha Duttagupta[b] Girish Phatak,*[a]

Received (in XXX, XXX) Xth XXXXXXXXX 20XX, Accepted Xth XXXXXXXXX 20XX
DOI: 10.1039/b000000x

The effect of Glycine Nitrate Precursor (GNP) synthesis parameters, *viz.* fuel to oxidant molar ratio, oven temperature during combustion, calcination temperature and calcination dwell time on the structural, morphological and electrical properties of nano crystalline Gadolinium doped Ceria (GDC) is reported in this paper. The X-ray diffraction studies confirm FCC crystal structure with lattice parameter 5.4230 (±0.5) Å under all conditions. Raman spectroscopy confirms FCC crystal structure with F_{2g} symmetry. Depending upon preparation conditions crystallite size between 15-40nm is obtained, which is confirmed by TEM images. Good crystallinity, lower lattice strain and optimum crystallite size distribution that results in high ionic conductivity at stoichiometric and slightly above stoichiometric F/O ratio (1.7 to 2.5) indicates that high adiabatic reaction temperature is of paramount importance. Oven temperature below 250°C during combustion reaction provides insufficient heat of formation and causes slow combustion reaction and results in lattice strain and low crystallinity. Higher oven temperatures also cause low crystallinity and lower crystallite size, indicating 250 °C is an optimum oven temperature. The calcination temperature of 900 °C provides high crystallinity, low stress and high ionic conductivity, probably due to optimum oxygen vacancies. The appropriate calcination dwell time is 8 hrs, although its influence on ionic conductivity is low. Good density of 94% of the theoretical density was obtained for pellets sintered at relatively low sintering temperature of 1350 °C for 8 hrs at F/O ratio of 1.7, oven temperature of 250 °C, calcination temperature of 800 °C with 8 hrs dwell time. These dense GDC pellets had average grain size of 0.4-3 μm and show promising ionic conductivity of 9.7×10^{-3} S. cm^{-1} at 700 °C. Activation energy calculated using Arrhenius plots shows values as low as 0.19± (0.01) eV, which is also the lowest reported value for GDC.

Introduction

Solid oxide fuel cells (SOFC) are amongst the most promising clean energy sources capable of high power generation (1-100 kW) with highest fuel efficiency (60-70%). It offers good fuel flexibility and moderate power density (200-300 mW. cm^{-2}) but at high operating temperature in the range of 1000 °C, which limits its use to stationary applications. [1, 2] Additionally, high operating temperature leads to significant difficulties in its sealing and interconnects. The need for such high operating temperature arises mainly out of the need to have reasonable ionic conductivity through the electrolyte. Presently, 20 mole % Yttrium stabilized Zirconia (YSZ) is commonly used in commercial SOFCs as electrolyte. The ionic conductivity of 0.1 S. cm^{-1} at 1000 °C for YSZ is seen as a benchmark. [3-5] Any attempt to lower the operating temperature through new electrolyte material development must aim at matching this value. [6]

Some of the new electrolyte materials under investigation, such as, for example, 8% Yttrium doped Zirconia (8mole% YSZ), Strontium and Magnesium doped Lanthanum Gallate (LSGM) or Gadolinium or Samarium doped ceria show reasonable ionic conductivity in the range 0.04-0.08 S. cm^{-1} at intermediate operating temperatures *i.e.* between 600-800°C.[7] However, Zirconia based electrolytes require very high sintering temperatures and have high internal resistance when operated below 700 °C.[6] LSGM faces lack of compatible cathode and anode materials, long-term chemical stability issues with some fuels and mechanical (high creep rate) issues compared to YSZ. On the other hand, doped ceria based electrolytes show promising ionic conductivities at intermediate operating temperatures. Even though its stability at reducing atmosphere remains serious concern, doped Ceria is among the best choices of electrolyte due to its high ionic conductivity at intermediate temperatures and good sinterability.[8] The stability issues can be tackled through a protective layer.[9]

Doped ceria crystallizes in Face centered cubic (FCC) crystal structure. Unlike perovskite structures, where oxygen hopping takes place through the triangle formed by two octahedral and

hexagonal sites, the oxygen ion hopping in doped ceria takes place across the edge of the lattice.[7, 10] Gadolinium and Samarium doped ceria (GDC and SDC, respectively) are amongst the best candidates for oxygen ion conduction in the intermediate temperature range (600-800 °C).[11] The ionic conductivity recorded for GDC and SDC is 4.7×10^{-2} S. cm^{-1} and 4.0×10^{-2} S. cm^{-1} at 700 °C respectively, which are better than YSZ at these temperatures. [12, 13] Gd^{3+} is a preferred dopant compared to Sm^{3+} in CeO_2 at low operating temperatures due to the closeness of its ionic radii to the critical radius for Ce^{4+} ion that results in lowering of average migration enthalpy and activation energy.[14] These advantages have propelled further investigations into GDC for Intermediate temperature solid oxide fuel cells (ITSOFC).

GDC is synthesized by various physical and chemical methods, such as, solid state reaction, pulsed laser deposition (PLD),[15] Aerosol-assisted metal-organic chemical vapor deposition (AA-MOCVD), oxalate co-precipitation, sol-gel,[16] hydrothermal treatment,[17] acetylacetonate precursors method, [18] diamine-assisted direct co-precipitation method, [19] spray pyrolysis, citric acid assisted precursor method, carbonate co-precipitation process [20] and modified gel casting method [21, 22]. The ionic conductivity of GDC by these methods lies between 0.008 to 0.024 S. cm^{-1} at 700 °C. GDC prepared by modified gel casting route has reported highest ionic conductivity about 0.046 S. cm^{-1} at 700 °C when sintered at 1450 °C.[23]

Combustion synthesis is one of the most frequently used synthesis method for GDC, especially with Glycine as fuel. [11, 24-26] The glycine nitrate precursor (GNP) method is very simple and fast process to prepare nano materials based on combustion of solid fuel and oxidants in form of nitrates. Prasad *et al* studied effect of the glycine content on the crystallite size, particle size, surface area, and sintered density by varying F/O ratio in the range of 0.1-0.55 moles of glycine. This paper reported 97% density at 1200 °C sintering temperature and ionic conductivity of 0.02 S. cm^{-1} at 600 °C. Jadhav *et al* synthesized $Ce_{0.9}Gd_{0.1}O_{1.95}$ using F/O ratio in the range of 1.1-1.9 and reported 90% sintered density at 1200 °C sintering temperature. Matović *et al* report effect of Gd doping on lattice parameter of $Ce_{1-x}Gd_xO_{1.95}$, where, x varied from 0-0.2. The F/O ratio for this study was 0.5 mole. Bošković *et al* also used Glycine nitrate synthesis method to study effect of simultaneous doping of Gd, Sm, and Y on lattice parameters, phase, sintering density and ionic conductivity. It is seen that these reports do present synthesis results, but their focus is mainly upon the sintering activities and their effect on ionic conductivity of GDC. Detailed study of synthesis parameters is missing in these reports.

The focus of this paper is to study the GDC preparation by Glycine nitrate precursor (GNP) method comprehensively. There are four important synthesis parameters in this method, *viz.* fuel to oxidant molar ratio (F/O), oven temperature during combustion, calcination temperature and calcination dwell time. The effect of these preparation parameters on the materials properties of GDC have been studied with the help of chemical, structural, morphological analysis. Sintered pellets of these GDC powders have been subjected to impedance measurements in the intermediate range of temperature (500 -700 °C) and correlated with the materials properties. The impedance analysis study is used to find individual contributions to ionic conductivity and the results are explained through Nyquist and Bode plots. These efforts have helped in identifying optimum preparation conditions for GDC that produce improved ionic conductivity.

Experimental Procedure

Gadolinium doped Ceria was prepared by the Glycine Nitrate Precursor (GNP) method using Cerium nitrate ($Ce(NO_3)_3$. 6 H_2O) and Gadolinium nitrate ($Gd(NO_3)_3$. H_2O) (Sigma Aldrich) as source of metal cations and Glycine (SISCO make) as fuel. The precursor was prepared by adding metal nitrates in molar stoichiometric proportion to fresh DI water (Millipore, Elix 3). Glycine was added directly in its solid form to have Fuel to

Parameter studied	Parameter levels or values	Fixed values of other parameters
Fuel to Oxidant (F/O) ratio	0.5, 1.0, 1.5, 1.7, 2.0, 2.5,3.0	Combustion temp.: 250 °C Calcination Temp.: 600 °C Calcination Dwell time: 2 hrs
Combustion temperature (°C)	150, 200, 250, 300, 350	Fuel to Oxidant Ratio: 1.7 Calcination Temp.: 600 °C Calcination Dwell time: 2 hrs
Calcination temperature (°C)	600, 700, 800, 900	Fuel to Oxidant Ratio: 1.7 Combustion Temp.: 250 °C Calcination Dwell time: 2 hrs
Calcination dwell time (hrs)	4, 8, 12	Fuel to Oxidant Ratio: 1.7 Combustion Temp.: 250 °C Calcination Temp.: 600°

Table 1: Table indicating parameters and their levels studied for synthesis of Gadolinium doped ceria (GDC) by combustion method

Oxidant (F/O) molar ratio varying from 0.5 to 3.0 in steps of 0.5. It may be noted that the stoichiometric molar ratio of Glycine to Gd and Ce nitrate is 1.7. Therefore, all other parameters *viz.* the oven temperature for combustion, calcination temperature and calcination dwell time were studied at a fixed molar fuel ratio of 1.7. The parameters which were studied and the values at which the studies were undertaken, are presented in Table 1.

The above mentioned mixture of precursor was then stirred for 12 hrs followed by its gelation in oven at 70 °C. Once the gel was formed, the combustion was set off in an oven at temperatures varying from 150-350 °C. After combustion, a pale yellow colored ash was collected, which was calcined at varying temperatures and dwell times (refer to Table 1) to obtain pure GDC. The calcined powders were characterized by X-ray Diffraction (XRD; PANanalytical PW3040/60 X'pert PRO diffractometer with CuKα target), RAMAN spectroscopy (BRUKER RFS 27; Standalone FT-Raman Spectrometer), tunneling electron microscope and selected area electron diffraction (TEM and SAED; PHILIPS CM200), particle size analysis (The Nicomp 380DLS; Particle sizing system) and Brunauer, Emmett and Teller (BET) surface area analysis (Quantachrome Nova1200 Surface area analyzer). Pellets of the as-prepared GDC powders were pressed by applying coaxial pressure of 285 MPa and were sintered at 1350 °C with ramp rate of 2 °C. min^{-1} and dwell time of 8 hrs at peak temperature. The density of the pellets was measured by weight and volume method and compared with the theoretical density of GDC, which is 7.24 g. cm^{-3}. [27, 28] The microstructure of the pellets was studied by Field Effect Gun Scanning Electron Microscope (FEG-SEM; The Quanta 200 FEG). Electrical contacts on both faces of the pellets were prepared by applying Platinum paste (Heraeus CL-11

7589, USA) followed by firing at 1000 °C peak temperature in order to prepare samples for impedance measurement. The impedance measurements were carried out using Potentiostat / Galvanostat (Autolab PGSTAT 100) at frequency perturbation between 1Hz to 1MHz and in the temperature range of 500-700 °C. The fired pellets were diced in beam using diamond cutter (ADT Dicing machine) and polished. The 3D X-ray topographic (Xradia MicroXCT-400) images were obtained to study the microstructure of the pellets in the bulk.

Results and Discussion

It is known that the molar ratio of fuel to metal nitrate precursor plays an important role in the combustion reactions. This ratio controls the enthalpy of the reaction and, in turn, decides whether the reaction is smolder or flame type. Generally, fuel lean and rich ratios produce smolder reactions while flame is produced near the stoichiometric ratio.[29] Exactly as per this expectation, smolder type reaction was found to be occurring at lower and higher fuel ratios of 0.5, 2.5 and 3, while flame type reaction is found to be occurring at the intermediate fuel ratios. Obviously, the type of reaction will have an effect on the properties of the GDC material produced. Table 2 presents the reaction type observed at different fuel ratios, along with the crystallite size, lattice constant derived from the X-ray diffraction patterns, average agglomerated particle size and surface area measured for powders using BET technique. The discussion about particle size and surface area can be found further in the text.

Sample code	Fuel molar (F/O) ratio	Reaction type	Crystallite size nm	Lattice constant Å	Average agglomerate size D_{50} µm	Surface area (BET) m^2/g
A	0.5	Smolder	13.4	5.403	0.8	104.2
B	1.0	Flame	27.3	5.388	1.1	-
C	1.5	Flame	30.7	5.404	1.1	-
D	1.7	Flame	30.7	5.425	1.7	65.3
E	2.0	Flame	49.0	5.414	1.7	-
F	2.5	Smolder	35.0	5.426	3.4	48.2
G	3.0	Smolder	13.6	5.359	1.6	93.1

Table 2: Effect of fuel to precursor molar ratio (F/O) on the reaction type, crystallite size and lattice constant, Average agglomerated particle size at an combustion temperature of 250 °C and calcination temperature and dwell time is 600 °C for 2 hrs

Figure 1 presents X-Ray Diffraction (XRD) patterns of GDC at different F/O ratios. Firstly, the XRD spectra confirms formation of GDC in fluorite FCC crystal structure with *Fm3m* symmetry that matches well with the JCPDS data (card no. 01-075-0162) for $Ce_{0.8}Gd_{0.2}O_{1.9}$. It is observed from the XRD patterns that the peak intensity increases with increasing F/O ratio up to 2.5 and decreased at higher F/O ratio of 3. The peak broadening is found to have decreased with increasing F/O ratio up to 2.5, which increased again for the F/O ratio of 3. Further, all diffraction peaks show a shift towards lower diffraction angles with increasing in F/O ratio up to 1.7, and it is close to the reported value ($2\theta = 28.50^{o}$) in the JCPDS data file. The changing peak width and shifts in the diffraction angle provides information about the crystallite size and lattice constant of this FCC type crystal structure. Figure 2 presents the crystallite size calculated from the Debye-Scherer equation and lattice constant calculated from the diffraction angle of the highest XRD peak. It is seen from this figure and Table 2 that the lowest crystallite size of about 13.4 nm is observed at a F/O ratio of 0.5, which increases and reaches a maximum value of about 49 nm at a F/O ratio of 2.0, and decreases again to 13.6 nm at the fuel of 3.0 moles. On the other hand, the lattice constant is found to be lower than that the standard value reported in JCPDS files (5.4230 Å) at lowest and highest F/O ratio (0.5 and 3.0) while matching with this value at the intermediate F/O ratios. The average agglomerated particle size (D_{50}) found from particle size measurements shows increase from 0.8 µm to 3.4 µm with increasing F/O ratio from 0.5 to 2.5, which reduced to 1.6 µm at F/O ratio 3.0. The particle size distribution is seen to be broader at stoichiometric F/O ratio, while it is relatively skewed at lower and higher D_{50} values. Correspondingly, the surface area of the powders shows decrease in surface area with F/O ratio up to 2.5, which further increases for fuel rich reaction or F/O ratio 3.0. Overall, range of surface area of the powder was observed between 48.2 $m^2.g^{-1}$ to 104.2 $m^2.g^{-1}$. It is seen that highest surface area is observed for the powders synthesized by smolder type of reactions except at F/O ratio 2.5. This aspect is discussed further.

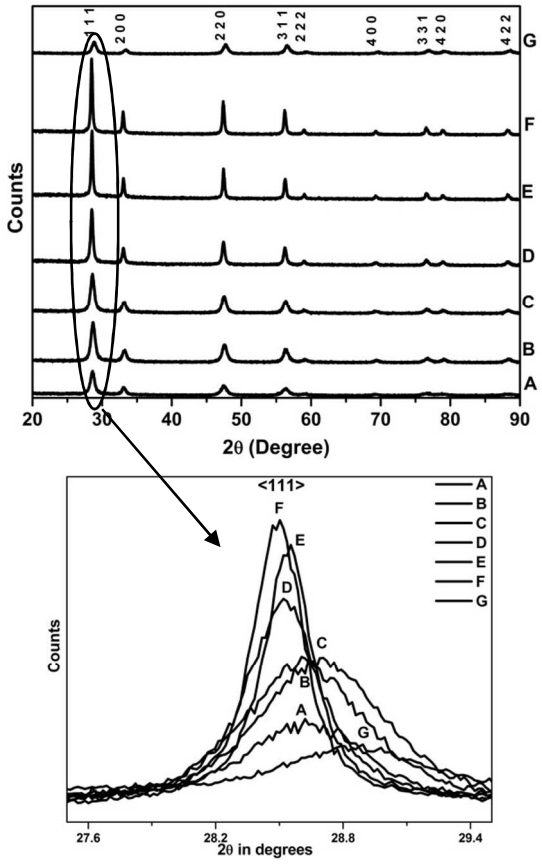

Figure 1: XRD pattern for Gadolinium doped ceria for different molar ratios of glycine (a) 0.5, (b) 1.0, (c) 1.5, (d) 1.7, (e) 2.0, (f) 2.5, (g) 3.0 after calcination at 600 °C for 2 hrs

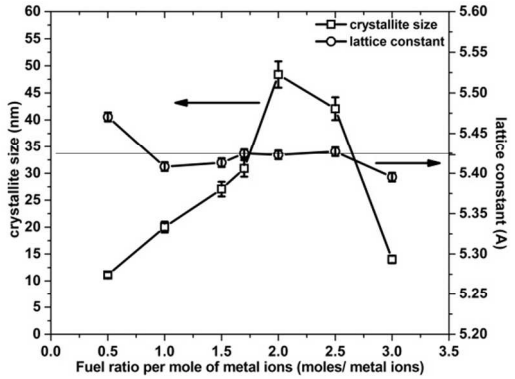

Figure 2: Effect of different fuel ratios per mole of metal nitrates on crystallite size and lattice constant of GDC

The above data indicates that the F/O ratio has profound influence over the resulting GDC material. It is seen that the smolder type reaction on either extremes of the F/O ratio produces lower crystallinity due to lower heat of formation of product. The crystallinity is high between F/O ratios 1.7 and 2.5, which allow higher energy generation due to higher adiabatic flame temperature produced during the reaction. This also reflects in peak position shifts, if any. It is seen that the peak positions and lattice parameters match well with the JCPDS data when the F/O ratio is closer to stoichiometric ratio, indicating low lattice stress for these combustion reactions. On the other hand, both the parameters (lattice parameters and crystallite size) show lower values for either extremes of F/O ratio, while peaking at the ratio of 2. It is reported that the smolder type reactions produce smaller crystallite sizes with narrower distribution due to slow adiabatic reaction. On the other hand, the flame type reactions, due to short reaction time, produce wider particle size distribution.[30] The increased average agglomerate particle size attributed to increase of flame temperature during combustion reaction.[31, 32] Hence, the lowest D_{50} vales are observed in case of smolder reactions. The surface area of the powder was also observed to be decreased in case of stoichiometric reaction due to high energy liberated in case of flame type reactions. The additional heat produces during such reactions assist agglomeration of the particles to increase in crystallite size and reduced surface area. In case of smolder reactions, release of huge amount of gases confine particle growth resulted in smaller crystallites and hence, larger surface area.[29, 32] This can be seen from Table 2. The reaction at F/O ratio of 2.5 is smolder type, but due to very high adiabatic flame temperature observed in this case, GDC produced in this reaction is highly crystalline, larger average agglomerated particle size with lowest surface area and has low built-in stress, as the lattice constant matches with the JCPDS data. The above results indicate that the released energy during the combustion reaction is paramount, which may or may not show off as flame or smolder type.

It is known that the heat supplied in terms of oven temperature for the combustion reaction changes the enthalpy of reaction, in turn influencing the combustion rate and physical properties of the GDC powders produced. In order to the study effect of oven temperature during combustion, the F/O ratio was kept constant

Oven temperature (°C)	Heat of formation of product $-\Delta H_r$ (kJ. Mol^{-1})	Crystallite size (nm)
150	122.79	49.0
200	277.77	35.0
250	991.34	30.6
300	805.63	22.2
350	399.66	17.5

Table 3: Oven temperature dependence of Heat of formation of product and crystallite size of Gadolinium doped Ceria synthesized by Glycine nitrate method

at stoichiometric ratio of 1.7, the gelation temperature at 70°C and calcination temperature at 600 °C for 2 hrs. The XRD patterns for these powders after combustion and after calcination are presented in Figure 3, while Table 3 presents the heat of formation of the product and the crystallite sizes for the corresponding oven temperatures. The heat of formation has been calculated from the difference between the measured temperature inside the beaker and the oven temperature, and by following the method described elsewhere. [31] It was observed that at temperatures below 250 °C, the reaction was slow and smolder type while flame type combustion takes place at 250 °C and above. It is seen from the XRD patterns that the peak intensity increases up to 250 °C oven temperature, and reduces thereafter. Equally, the peaks shift to the standard 2θ value up to 250 °C and shift to lower values again at higher temperature. These observations explain the increasing crystallinity and shift towards expected 2θ values for GDC material up to 250 °C.

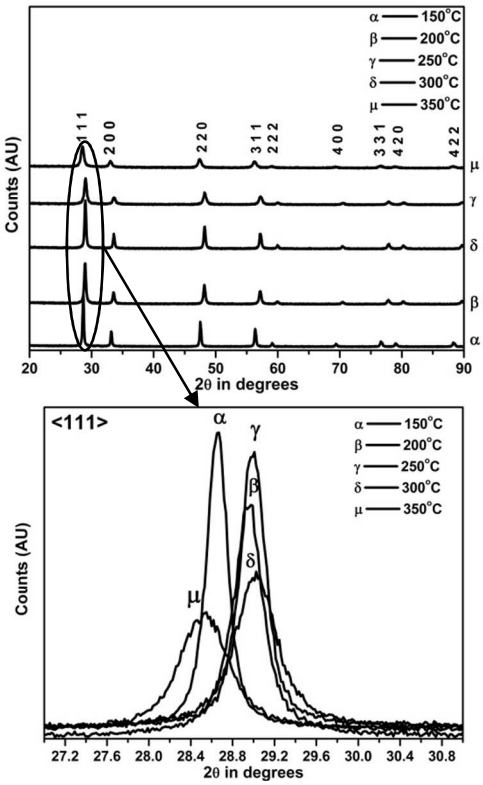

Figure 3: XRD patterns of powder prepared at different oven temperatures having F/O ratio 1.7 and calcined at 600 ˚C for 2 hrs

The peak width measurements indicate that crystallite size of the powder decreases continuously with increasing oven temperature. It is reported that the oven temperature influences the reaction time of combustion, which reduces with increasing oven temperature.[33] Clearly, the shortening of time available for crystallite formation with increasing oven temperature causes reduction in the crystallite size.

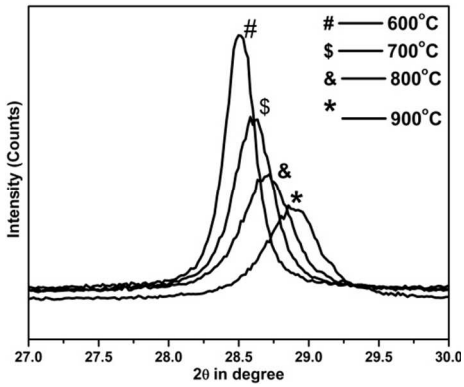

Figure 4: Magnified image of highest XRD peak showing shift and intensity variation with respect to calcination temperature

Calcination temp. (°C)	Lattice const. (Å)	Crystallite size (nm)	Shift in peak position w. r. t. std. JCPDS value (2θ)	Lattice strain [%]
600	5.348	24.5	0.41	0.71
700	5.389	22.3	0.18	0.63
800	5.397	32.7	0.14	0.38
900	5.423	35.0	0.00	0.04

Table 4: Effect of calcination temperature on lattice constant, crystallite size, peak position and lattice strain calculated by XRD pattern

Figure 4 presents comparison of the highest intensity peak in the XRD patterns for powders with calcination temperatures from 600 to 900 °C. These experiments were carried out at F/O ratio of 1.7, oven temperature for combustion 250 °C and calcination dwell time 2 hrs. It is seen that this highest intensity peak *viz.* the <111> peak, shifts towards the standard 2θ value with increasing calcination temperature. This causes increase in the lattice constant with calcination temperature. Table 3 presents the measured shift in the 2θ values along with the lattice constant at different calcination temperatures, which confirms this observation. It is also seen from the XRD patterns that the peak intensity increases with increasing calcination temperature. Thus, the crystallinity of the calcined powders increased with calcination temperature while the built-in stresses decreased. Table 4 also presents the change in crystallite size with calcination temperature. Expectedly again, the crystallite size is found to be increasing with calcination temperature, reaching to about 35 nm at 900 °C. Reduction of stress, increase in crystallinity and an increase in lattice parameter along with crystallite size due to calcination temperature has been reported earlier in the literature in case of GDC as well as Ceria and also in some of combustion reactions [20, 34-36]. It is also known that pre-existing compressive stress in nano materials reduces during calcination process. This is attributed to increase in diffusion rate of oxygen with increasing calcination temperature for GDC.[37] Such increase in d-spacing lowers the lattice strain due to reduction in atomic vacancies as explained by Shidong Li *et al*. [38] This decrease in lattice strain with calcination temperature can be observed in Table 4, which is seen to be lowest at 900 °C. In fact, the lattice parameter is found to be equal to JCPDS values (~5.423 Å) at 900 °C. The studies of calcination temperature are important because increasing oxygen diffusion with increasing calcination temperature is expected to affect the oxygen vacancies, and in turn, influence the ionic conductivity. Conductivity measurements on samples calcined above 900 °C have independently confirmed reduction in ionic conductivity.

Calcination dwell time (hrs)	Lattice constant (Å)	Shift in peak position w. r. t. std. JCPDS value (2θ)	Lattice strain [%]
2	5.315	0.60	0.31
4	5.412	0.07	0.23
8	5.398	0.15	0.16
12	5.386	0.21	0.40

Table 5: Effect of calcination dwell time on lattice constant, crystallite size, peak position and lattice strain calculated by XRD pattern

The effect of calcination dwell time was studied in the range of 2 to 12 hrs at calcination temperature 800 °C, and F/O ratio and oven temperature at 1.7 and 250 °C, respectively. All samples show pure FCC crystalline phase. Table 5 presents the data derived from XRD of samples with different calcination dwell time, *viz.* lattice constant, 2θ shift of the highest peak, and the lattice strain. From the Table, the <111> peak position is seen shifted towards lower 2θ value at dwell time of 2 hrs, which increases to the JCPDS value at 4 hrs dwell time, due to reduced stresses. Further increase in calcination dwell time up to 8 hrs dwell time shifted the <111> peak again towards higher 2θ values, reducing the d-spacing mostly through lowering of tensile stresses in lattice.

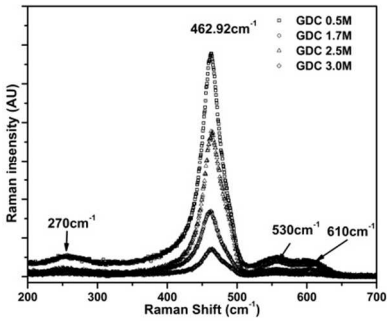

Figure 5: Raman spectra of GDC powders synthesized using different fuel molar ratios

Figure 5 presents the Raman spectra for GDC powders synthesized using F/O ratios 0.5, 1.7, 2.5 and 3. The spectrum confirms that GDC crystallizes in a single cubic phase having F_{2g} symmetry. The peak at 465cm^{-1} corresponds to F_{2g} phonon mode, the low intensity peaks observed around 510 cm^{-1} and 630 cm^{-1} describe oxygen vacancies corresponding to charge compensating defects, while the weak intensity peak around 270 cm^{-1} is attributed to second order Raman scattering. [39-41] The F_{2g} mode becomes slightly broader due to the increased strain. Phonon confinement, inhomogeneous strain and the presence of defects

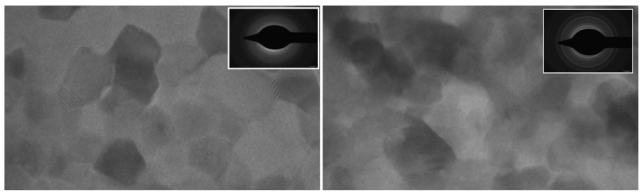

(a) (b)

Figure 6: TEM images of Gadolinium doped Ceria for fuel molar ratio (a) 1.7 Mole and (b) 3.0 Mole

due to non-stoichiometric F/O ratio cause the observed changes of the Raman spectra.[42] Further, red shift in these spectra observed in case of non-stoichiometric (fuel lean and rich) molar ratios clearly implies that smaller crystallite size compared to stoichiometric or close to stoichiometric molar ratios. [43] It is clearly observed that peak intensities vary with F/O ratio. Decrease in the peak intensity of F_{2g} mode is due to polarizability and concentration of Raman active groups.[44, 45]

Figure 6 presents the TEM image of GDC powders for stoichiometric (1.7) and fuel rich (3.0) F/O ratios. It is seen that stoichiometric combustion reaction has average particle size of the order of 15-40 nm and wide particle size distribution compared to fuel rich reaction. Fuel rich combustion reaction shows fine particles with particle size distribution in small range of 15-22 nm. Further, the stoichiometric F/O ratio has broader particle size distribution, with average particle size of 30 nm, while the fuel rich F/O ratio shows narrower size distribution with average particle size of 18 nm. This variation is due to the difference in the rate of combustion reaction, which is faster at F/O ratio 1.7 and slower at the ratio of 3.[46,47] The concentric rings in SAED shown in insets of confirm polycrystalline FCC crystal structure.

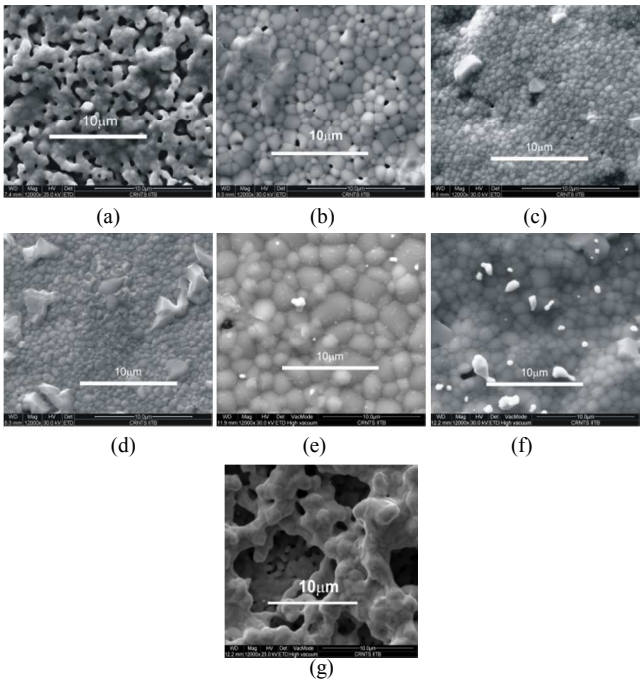

(a) (b) (c)

(d) (e) (f)

(g)

Figure 7: SEM images at 12000× of pellets prepared by powders with different fuel molar ratios (a) 0.5, (b) 1.0, (c) 1.5, (d) 1.7, (e) 2.0, (f) 2.5, (g) 3.0 and sintered at 1350 ˚C for 8 hrs

Figure 7 presents the surface morphology for pellets sintered at 1350 °C with dwell time of 8 hrs using powders synthesized with different F/O ratio ranging from 0.5 to 3. It is seen that pellets prepared at fuel lean conditions (a, b, c) exhibit lower grain size (~0.1-1 μm) and pinholes, resulting in lower density. Indeed, these pellets exhibit density of 79-85% of the theoretical density. The pellets with GDC material prepared at stoichiometric ratio and slightly above the stoichiometric ratio (d-f) showed grain growth of the order of 5 μm and pinhole free surface with density above 90 % of the theoretical density. Such a grain growth reduces resistance to the oxygen ion hopping across grain boundaries. This implies powders prepared with F/O ratio close to stoichiometric ratio improve density of pellet through grain growth during sintering process. In case of sample (g) the density is again lowered due to smaller crystallite size and narrow particle size distribution. Correspondingly, poor microstructure having large voids was observed in this case. Figure 8 represent 3D X-ray topographical image of the beam diced across thickness at center of pellets. The image showed cross sectional layer of the pellets (a), (d) and (g) shown in Figure 7. It is seen from figure that, the microstructure of the pellets in the center is similar to the surface of the pellets. The voids are spread all over the surface homogeneously. The voids are seen in large area in case of lower F/O ratio and moderate voids are seen on the samples prepared with fuel rich reactions. Sample prepared with stoichiometric F/O ratio on the other hand seen dense microstructure. Hence, it can be concluded from the topographical images that, the microstructure of the pellets in the bulk is similar of the pellets.

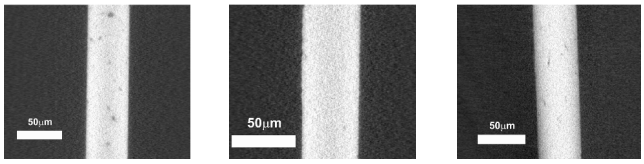

(a) (b) (c)

Figure 8: 3D X-ray topographic images of the central layer of the sintered pellets of GDC prepared with powders having different fuel molar ratios (a) 1.0, (b) 1.7, (c) 3.0

Figure 9 shows representative EIS frequency response using Nyquist plot for one of these pellets (sample F with F/O ration 2.5) measured at 700 °C in frequency perturbation of 1 Hz to 1 MHz. Two partial semicircles are observed in this frequency perturbation range. The high frequency semicircle implies contribution of grains to the impedance, while the low frequency semicircle represents grain boundary conduction process in GDC. The first semicircle is incomplete due to very small RC time constant values for the intra-grain ionic conduction at this temperature.[48] A depressed semicircle at low frequency confirms presence of constant phase element (CPE) instead of pure capacitance.[49] The nature of impedance spectra for all samples was similar. The inset in this figure shows the best-fit equivalent circuit with values of each element. Resistance R1 is series resistance representing resistance across the circuit. A parallel connection of constant phase element and resistance represents grain boundary, however the next parallel combination of CPE and resistance along with Warburg represents grains. The Warburg element included in equivalent circuit of grain region shows linear ionic diffusion in the grains.[50] Table 6 presents the grain and grain boundary conductivity and activation energy of total conductivity derived from impedance curves for

all samples with various F/O ratios. It is observed from Table 6 that the ionic conductivity is superior for GDC prepared at close to stoichiometric ratios due to high crystallinity, larger and well developed grains with minimal stress and low grain boundary resistance.

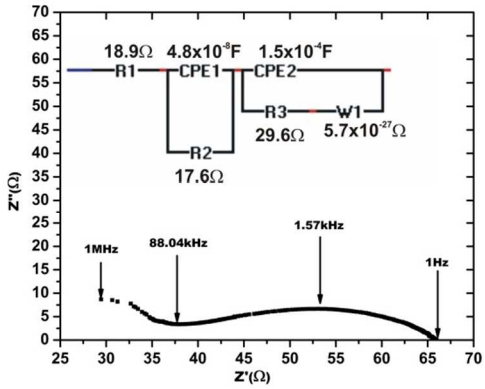

(a)

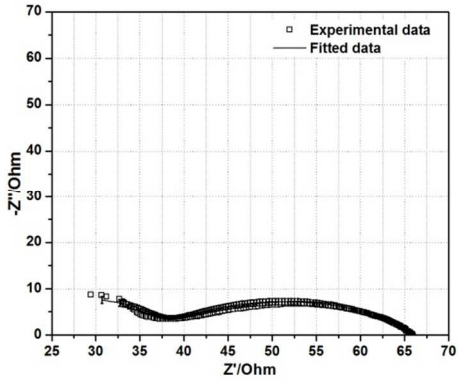

(b)

Figure 9: (a) Impedance spectra of sintered sample (F) at 1350 ˚C measured at 700 ˚C (b) equivalent circuit for fitted data with RMS value of fitting is 0.47 shown in inset of (a)

Sample	Grain conductivity S. cm^{-1}	GB conductivity S. cm^{-1}	Total Conductivity S. cm^{-1}	Activation energy (eV)
A	0.0008	0.0009	0.0004	0.352
B	0.0104	0.0056	0.0037	0.214
C	0.0135	0.0060	0.0042	0.195
D	0.0249	0.0158	0.0097	0.191
E	0.0122	0.0040	0.0030	0.341
F	0.0093	0.0054	0.0034	0.262
G	0.0064	0.0040	0.0025	0.314

Table 6: Grain conductivity, grain boundary conductivity and total conductivity for different molar ratios of fuel and oxidant ratio of glycine in GDC sintered at 1350 °C.

Figure 10 presents Arrhenius plot of Log (σT) versus 1000/T measured for all the pellets, where σ is total conductivity. All samples show temperature dependent ionic conductivity with varying activation energy between 0.19 and 0.35 eV. It is seen that the Activation energy is lowest for sample D (0.19 ±0.018 eV), which is synthesized by stoichiometric F/O ratio. Generally, it is seen that the fuel lean and rich reactions exhibit higher activation energies compared to stoichiometric reactions.

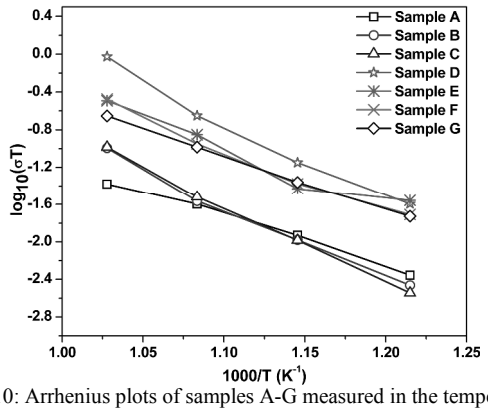

Figure 10: Arrhenius plots of samples A-G measured in the temperature range of 500-700 °C

Figure 11 presents dependence of phase angle between real and imaginary parts of impedance on F/O ratio. Frequency dependence of ionic charge transport can be more precisely described using Bode plot. The Bode plots presented in Figure 10

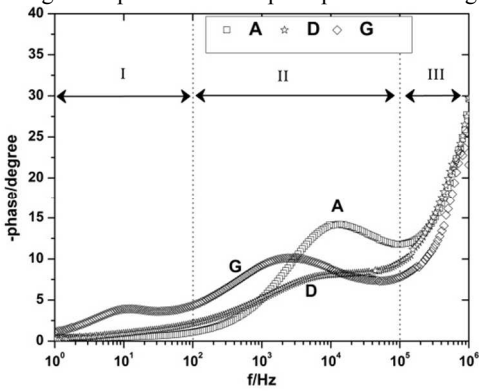

Figure 11: Bode plot of log f v/s phase angle for different molar ratios at 700 °C

can be separated in three different frequency regions, *viz.* (a) low frequency (1 Hz-1 kHz) (zone I) (b) intermediate frequency (1-100 kHz) (zone II) (c) high frequency (100 kHz-1 MHz) (zone III). The relaxation of phase observed in zone III is attributed to intra-grain charge transfer. These plots are indistinguishable in the given frequency range, probably due to smaller RC time constant as discussed earlier. Relaxation peak observed in zone II corresponds to charge transfer across grain boundaries.[51] The higher intensity relaxation peaks are observed for samples (A, G) in this region, where lower grain size results in more grain boundaries. The relaxation peak disappears in case of stoichiometric reaction (sample D), which is attributed to low resistance ionic transport across grain boundaries. There is no relaxation observed in Zone I for all samples except sample G (at 100 Hz), which attributed to charge transfer losses at electrode interface due to roughness of pellet surface.[52]

Figure 12 presents temperature dependence of total ionic conductivity plotted as Bode plots for sample D that shows highest ionic conductivity at 700 °C in the present investigation. The relaxation peaks corresponding to inter-grain charge transfer shift towards higher frequency with increase in temperature. This indicates that this relaxation is thermally activated and is attributed to lowering of impedance across grain boundary. The

relaxation peak intensities are also found to be decreasing with increasing temperature due to lowering in capacitive reactance across the grain boundaries.

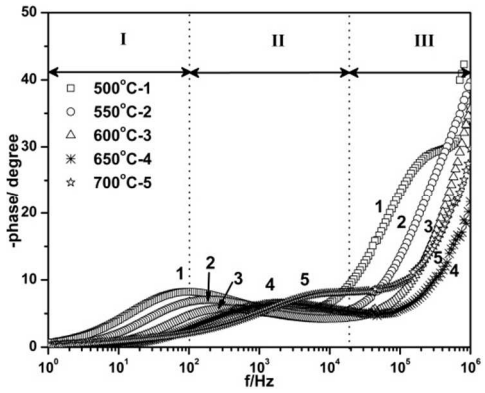

Figure 12: Temperature dependence of phase angle at different temperature ranging from 500-700 °C for pellet sintered at 1350 °C.

The ionic conductivity as a function of oven temperature is presented in Figure 13. The bulk ionic conductivity and intra grain conductivity is found to be highest at 250 °C oven temperature, possibly due to good grain growth and high pellet density of the order of 94%. This oven temperature was also found to have highest heat of formation of product (Table 2), which results in optimum crystallite sizes to obtain higher density. The ionic conductivity for oven temperature between 150-200 °C is found to be low compared to that at 250-350 °C. Low density of pellets (83-85%) in these temperature ranges explains these results well.

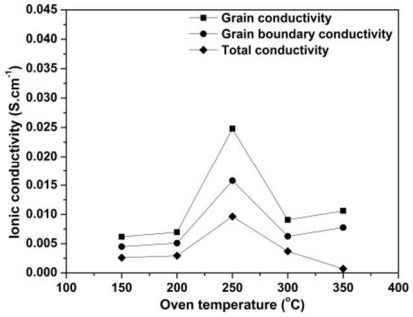

Figure 13: Grain and grain boundary conductivity of GDC powders combust at different temperature ranging from 150 °C to 350 °C.

Figure 14 presents the total ionic conductivity of pellets as a function of calcination temperature. It is seen from this figure that

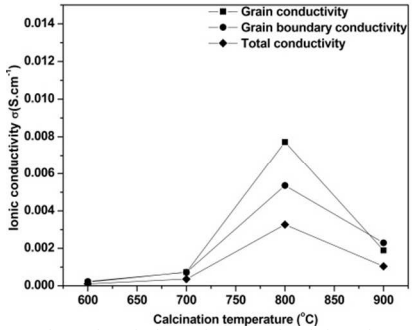

Figure 14: Grain and grain boundary conductivity of GDC powders calcined at different temperature ranging from 600 °C to 900 °C for dwell time 8 hrs.

the grain and grain boundary conductivity increases with calcination temperature up to 800 °C and then reduced further at 900 °C. This increase in grain conductivity and grain boundary ionic conductivity is attributed to better crystallization and higher density of the pellet respectively, at 800 °C. The lowering in ionic conductivity in case of powder calcined at 900 °C is due to lower oxygen vacancies and lower sintering density of pellet.

The calcination dwell time study has been done in the range of 2 hrs to 12 hrs at 800 °C. The results for grain, grain boundary and total conductivity are plotted against dwell time in Figure 15.

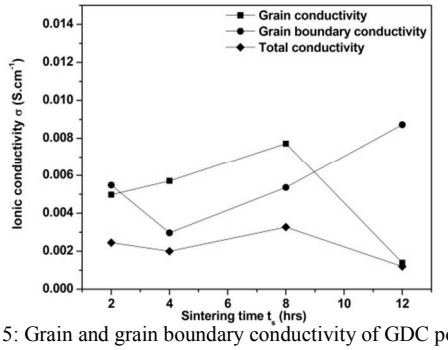

Figure 15: Grain and grain boundary conductivity of GDC powders calcined at 800 °C with different dwell times ranging from 2 hrs -12 hrs.

In general, the overall grain conductivity is seen increasing with calcination dwell time up to 8 hrs and decrease thereafter. The grain and grain boundary contribution is seen to be moving in opposite direction at high dwell time of 12 hrs. The improved grain boundary conductivity may be due to reduced defects at the interface, the reduced grain conductivity may points towards possible reduction in oxygen vacancies. In general, however, the effect of calcination dwell time is found to be limited.

It can be summarized from above study that there are three main factors that can extract maximum ionic conductivity form an electrolyte at lower temperatures. First, optimum oxygen vacancies, second, loss-free grains and grain boundaries and finally, lower activation energy. From the exhaustive experimental data presented here, it is seen that stoichiometric or slightly above stoichiometry reactions (F/O ratio 1.7 to 2.5) are more favorable for high crystallinity and achieving better sintered density. This is due to broader particle size distribution caused by faster and high energy adiabatic reactions at these F/O ratios. This is also corroborated from the TEM images and blue shifts in Raman analysis. The calcination temperature greatly affects crystallinity, the built-in tensile / compressive strain in the nano range particles and oxygen vacancies within the grains. Higher calcination temperature causes better crystallinity but beyond a limit reduces the oxygen vacancies. Therefore, the calcination temperature must be optimum to maintain appropriate oxygen vacancies and better crystallinity. Enthalpy of reaction or heat of formation of product is a function of oven temperature during combustion *i.e.* the heat supplied for combustion. An intermediate oven temperature of 250 °C for given F/O ratio results in appropriate crystallite and particle size distribution, which, in turn results in improved grain and grain boundary structure, as reflected from grain and grain boundary conductivity. Thus, it can be concluded that strain free broad particle size distribution favors dense grain structure with small grain boundary region and results in superior ionic conductivity. Appropriate oxygen vacancy creation in the grains helps in

improved conductivity and lowering of activation energy.

Conclusions

In this study we have prepared nano crystalline Gadolinium doped Ceria (GDC) by glycine nitrate precursor method. The influence of important synthesis parameters, such as, fuel to metal nitrate (oxidant) ratio or F/O ratio, oven temperature for combustion, calcination temperature and calcination dwell time on the resulting crystal structure, microstructure, lattice parameter and ionic conductivity have been studied in a finite range of their values. It is seen that the F/O ratio, oven temperature during combustion and calcination temperature influence the crystallite size, particle size, lattice strain within the grains and particle size distribution of the resulting GDC powders, eventually influencing the ionic conductivity of the sintered pellets. This study underlines the importance of studying preparation parameters in order to obtain better materials properties, which eventually guide towards selection of optimum synthesis parameters for better ionic conductivity of GDC. Under such conditions, an ionic conductivity of 9.7×10^{-3} S. cm^{-1} has been achieved at 700 °C operating temperature. This ionic conductivity value is highest for pellets sintered at 1350 °C sintering temperature. An activation energy calculated for best sample (sample D) was as low as 0.19 (±0.01) eV, which is also the lowest activation energy reported so far.

Acknowledgements

Authors are very thankful to C-MET for providing all experimental facilities. Authors are also thankful to INUP, IIT, Bombay (IITB) and SAIF, IITB for providing several characterization facilities. The authors express their gratitude towards Department of Electronics and Information Technology (DeitY), and National Programme on Micro and Smart Systems (NPMASS), Govt. of India, for providing financial support to Mr. S. G. Kulkarni.

References

1. B. C. H. Steele, Philosophical Transactions of Royal Society of London A, 1996, 354, 1695-1710
2. A. Bieberle-Hütter, D. Beckel, A. Infortuna, U. P. Muecke, J. L.M. Rupp, L. J. Gauckler, S. Rey-Mermet, P. Muralt, N. R. Bieri, N. Hotz, M. J. Stutz, D. Poulikakos, P. Heeb, P. Müller, A. Bernard, Journal of Power Sources, 2008, 177, 123-130.
3. A. Mineshige, T. Nakao, Y. Ohnishi, R. Sakamoto, Y. Daiko, M. Kobune, T. Yazawa, H. Yoshioka, T. Fukutsuka, and Y. Uchimoto. Journal of the Electrochemical Society, 2010,157, B1465-B1470
4. J. B.Goodenough, Report on Progress in Physics, 2004, 67, 1915–1993.
5. H. Yokokawa, N. Sakai, T. Horita and K. Yamaji, Fuel Cells, 2001, 2, 117-131.
6. J. M. Ralph, A. C. Schoeler, M. Krumpelt, Journal of Materials Science, 2001, 36, 1161 – 1172.
7. V. V. Kharton, F. M. B. Marques, Ionics, 2001, 11, 321-326.
8. D. H. Prasad, H. R. Kim, J. S. Park, J. W. Son, B. K. Kim, H. W. Lee, J. H. Lee, Journal of Alloys and Compounds, 2010, 495, 238–241.
9. A. Tomita, Y. Tachi, T. Hibino, Electrochemical and Solid-State Letters, 2008, 11, B68-B70.
10. L.S.M. Traqueia, F.M.B. Marques, V.V. Kharton, Boletin de la Sociedad Española de Cerámica y Vidrio, 2006, 45 [3], 115-121.
11. D. H. Prasad, J. W. Son, B. K. Kim, H. W. Lee, J. H. Lee, Journal of Ceramic Processing Research, 2010, 11, 176-183.
12. V. Gil, C. Moure , P. Durán, J. Tartaj, Solid State Ionics, 2007, 178, 359–365.
13. N. M. Sammes, G. A. Tompsett, Journal of American Ceramics Society, 1997, 80, 3181–86
14. B.C.H. Steele, Solid State Ionics, 2000, 129, 95–110.
15. J. L. M. Rupp, A. Infortuna, and L. J. Gauckler, Journal of American Ceramic Society, 2007, 90, 6, 1792–1797
16. R.O. Fuentes, R.T. Baker, International Journal of Hydrogen Energy, 2008, 33, 3480 – 3484.
17. S. Dikmen, P. Shuka, M. Greenblatt, H. Gocmez, Solid State Sciences, 2002, 4, 585–590.
18. L. L. Shaw, C. Shen, E. L. Thomas, Journal of Sol-Gel Science and Technology, 2010, 53, 1, 1-11.
19. E. Traversa, V. Esposito, Journal of American Ceramic Society, 2008, 91, 4, 1037–1051.
20. A. I. Y. Tok, L. H. Luo, F. Y. C. Boey, J. L. Woodhead, Journal of Materials Research, 2006, 21, 1, 119-124.
21. H. Deguchia, H. Yoshidaa, T. Inagakia, M. Horiuchi, Solid State Ionics, 2005, 176, 1817 – 1825.
22. H. Z. Song, H. B. Wang, S. W. Zha, D. K. Peng, G. Y. Meng, Solid State Ionics, 2003, 156, 249– 254
23. J. G. Cheng, S. W. Zha, J. Huang, X. Q. Liu, G. Y. Meng, Materials Chemistry and Physics, 2003, 78, 791–795.
24. L. D. Jadhav, M. G. Chourashiya, K. M. Subhedar, A. K. Tyagi, J. Y. Patil. Journal of Alloys and Compounds, 2008, 470, 383–386.
25. B. Matović, S. Bošković, L. Živković, M. D. Vlajić, V. D. Krstić, Materials Science Forum, 2005, 494, 175-180.
26. S. Bošković, S. Zec, G. Branković, Z. Branković, A. Devećerski, B. Matović, F. Aldinger, Ceramics International, 2010, 36, 121–127.
27. S. B. Bošković, D. R. Djurovic, S. P. Zec, B. Z. Matovic, M. Zinkevich, F. Aldinger, Ceramics International, 2008 , 34, 2001–2006.
28. S. Lübke, H. D. Wiemhöfer, Solid State Ionics, 1999, 117, 229–243.
29. X. Guo, D. Maob, G. Lu, S. W., G. Wu, Journal of Catalysis, 2010, 271, 178–185.
30. K. C. Patil, S. T. Aruna, T. Mimani, Current Opinion in Solid State and Materials Science, 2002, 6, 507–512.
31. A. B. Salunkhe, V. M. Khot, M. R. Phadatare, S. H. Pawar, Journal of Alloys and Compounds, 2012, 514, 91– 96.
32. C.S. Naveen, M.L. Dinesha, H.S. Jayanna, J. Mater. Sci. Technol., 2013, 29, 898 - 902
33. A. Alves, C. P. Bergmann, F. A. Berutti, Novel Synthesis and Characterization of Nanostructured Materials, Springer-Verlag Berlin Heidelberg, 2013. 978-3-642-41275-2.
34. V. N. Morris, R. A. Farrell, A. M. Sexton, M. A. Morris, Journal of Physics: Conference Series, 2006, 26, 119–122.
35. M. T. Makhlouf, B. M. Abu-Zied, T. H. Mansoure. Hindawi Publishing Corporation, Journal of Nanoparticles, 2013,

384350, 1-7
36. T. Surendar, S. Kumar, V. Shanker, Phys. Chem. Chem. Phys., 2014, 16, 728-735
37. S. Mahmud, R. K. Sendi, Journal of Physical Science, 2013, 24, 1–15
38. S. Li, M. S. Sellers, C. Basaran, A. J. Schultz and D. A. Kofke, Int. J. Mol. Sci., 2009, 10, 2798-2808.
39. Y. Ji, J. Liu, T. He, J. Wang, W. Su, Journal of Alloys and Compounds, 2005, 389, 317–322.
40. R. C. Maher, L. F. Cohen, P. Lohsoontorn, D. J. L. Brett, and N. P. Brandon, J. Phys. Chem. A, 2008, 112, 1497-1501.
41. S. Askrabic, R. Kostic, Z. Dohcevic-Mitrovic, Z. V. Popovi, Journal of Physics: Conference Series, 2007, 92, 012042.
42. N. Paunovic, Z. Dohcevic-Mitrovic, R. Scurtu, S. Askrabic, M. Prekajski, B. Matovic, Z. V. Popovic, Nanoscale, 2012, 4, 5469–5476.
43. E. C. C. Souza, E. N. S. Muccillo, Journal of Alloys and Compounds, 2009, 473, 560–566.
44. H. Vašková, International Journal of Mathematical Models and Methods in Applied Sciences, 2011, 5, 7, 1205-1212.
45. G. E. Walrafen, J. Chem. Phys., 1967, 46, 5, 1870-1878.
46. K. C. Patil, M. S. Hegde, T. Rattan, S. T. Aruna, Chemistry of Combustion Synthesis, Properties and Applications nanocrystalline Oxide Materials. Singapore : World Scientific Publishing Co. Pte. Ltd., 2008.
47. R. R. Kondakindi, Indian Journal of Chemistry, 2012, 51, 931-936.
48. K. Huang, M. Feng, J. B. Goodenough, Journal of American Ceramic Society, 1998, 81, 357–362
49. P. Muralidharan, S. H. Jo, D. K. Kim, Journal of American Ceramic Society, 2008, 91, 3267–3274
50. E. Barsoukov, J. Ross Macdonald. Impedance Spectroscopy, Theory, Experiment, and Applications. New Jersey : A John Wiley & Sons, Inc., Publication, 2005.
51. M. E. Orazem, B. Tribollet, Electrochemical Impedance Spectroscopy. New Jersey: A John Wiley & Sons, Inc., Publication, 2008.
52. S. Song, P. Xiao, Materials Science and Engineering, 2003, B97, 46-53.

[a] *Centre forMaterials for Electronics Technology (C-MET), Panchawati, Pune, INDIA. Fax:+912025898141; Tel:+912025899173; E-mail: gjp@cmet.gov.in*
[b] *Department of Electrical Engineering,Indian Institute of Technology, Bombay (IITB), Mumbai, INDIA. Fax: +912225723707; Tel: +912225767866; E-mail: sdgupta@ee.iitb.ac.in*

